measurements were very difficult because of the buildup of a photothermal background over long illumination times by the pump beam [the probe had no noticeable effect on this buildup (figs. S6 to S8) (*17*)].

We could not observe simultaneous fluorescence and photothermal signals from the spots of Fig. 2. Such simultaneous signals arose only from abnormally bright spots, attributable to large aggregates, and showed quick correlated decays of both signals upon illumination (fig. S9) (*17*). On the sample of Fig. 2, we also observed a few spots with strong photothermal signals corresponding to an absorption cross section of about 1 nm^2, which shows one-step bleaching. Possible interpretations are aggregates of several molecules desorbing simultaneously or, more probably, another chemical species with a large absorption cross section, possibly with excited-state absorption of the intense probe beam. We only found very few examples of two-step photobleaching of the BHQ1-10T-BHQ1 constructs. We believe that this absence results from the low probability of bleaching, joined with the low probability of finding two favorable orientations in the same construct.

Our successful single molecule detection relied here on favorable conditions, the use of glycerol (with large $\partial n/\partial T$ and poor heat conduction) instead of water, with a high heating power of 5.1 mW focused into the diffraction-limited spot and with an even higher probe power of more than 70 mW. Although the conditions for single-molecule absorption in a cell, for example, would be far from these ideal ones, this result opens the way for further optimization of the technique and to a much broader variety of absorbing molecules. Interesting candidates are natural absorbers, for example, metal proteins such as hemoglobin, which would be useful for applications in analytical biochemistry and medical assays (*24*).

An intrinsic limitation of the photothermal method is the low transduction factor between pump and probe because of the relatively weak variation of refractive index with temperature. A future search for more-efficient transduction, for example, photomechanical or photoelectrical detections using micro- and nano-optomechanical systems (*25*), appears full of promise.

References and Notes

1. W. E. Moerner, M. Orrit, *Science* **283**, 1670 (1999).
2. M. Orrit, J. Bernard, *Phys. Rev. Lett.* **65**, 2716 (1990).
3. R. A. Keller *et al.*, *Appl. Spectrosc.* **50**, 12A (1996).
4. W. E. Moerner, L. Kador, *Phys. Rev. Lett.* **62**, 2535 (1989).
5. L. Kador, T. Latychevskaia, A. Renn, U. P. Wild, *J. Chem. Phys.* **111**, 8755 (1999).
6. J. Y. P. Butter, B. Hecht, B. R. Crenshaw, C. Weder, *J. Chem. Phys.* **125**, 154710 (2006).
7. I. Gerhardt *et al.*, *Phys. Rev. Lett.* **98**, 033601 (2007).
8. M. Tokeshi, M. Uchida, A. Hibara, T. Sawada, T. Kitamori, *Anal. Chem.* **73**, 2112 (2001).
9. D. Boyer, P. Tamarat, A. Maali, B. Lounis, M. Orrit, *Science* **297**, 1160 (2002).
10. S. Berciaud, L. Cognet, G. A. Blab, B. Lounis, *Phys. Rev. Lett.* **93**, 257402 (2004).
11. S. Berciaud, D. Lasne, G. A. Blab, L. Cognet, B. Lounis, *Phys. Rev. B* **73**, 045424 (2006).
12. J. Hwang, M. M. Fejer, W. E. Moerner, *Phys. Rev. A* **73**, 021802 (2006).
13. F. V. Ignatovich, L. Novotny, *Phys. Rev. Lett.* **96**, 013901 (2006).
14. G. Wrigge, J. Hwang, I. Gerhardt, G. Zumofen, V. Sandoghdar, *Opt. Express* **16**, 17358 (2008).
15. P. Kukura, M. Celebrano, A. Renn, V. Sandoghdar, *Nano Lett.* **9**, 926 (2009).
16. W. Min *et al.*, *Nature* **461**, 1105 (2009).
17. Materials and methods are available as supporting material on *Science* Online.
18. A. Gaiduk, P. V. Ruijgrok, M. Yorulmaz, M. Orrit, *Chem. Sci.* **1**, 343 (2010).
19. V. V. Didenko, Ed., *Methods in Molecular Biology: Fluorescent Energy Transfer Nucleic Acid Probes: Designs and Protocols* (Humana, Totowa, NJ, 2006).
20. S. A. E. Marras, F. R. Kramer, S. Tyagi, *Nucleic Acids Res.* **30**, e122 (2002).
21. M. A. van Dijk *et al.*, *Phys. Chem. Chem. Phys.* **8**, 3486 (2007).
22. C. F. Bohren, D. R. Huffman, *Absorption and Scattering of Light by Small Particles* (Wiley, New York, 1998).
23. A. Arbouet *et al.*, *Phys. Rev. Lett.* **93**, 127401 (2004).
24. S. Lu, W. Min, S. Chong, G. R. Holtom, X. S. Xie, *Appl. Phys. Lett.* **96**, 113701 (2010).
25. S. W. Stahl, E. M. Puchner, H. E. Gaub, *Rev. Sci. Instrum.* **80**, 073702 (2009).

26. We acknowledge financial support by European Research Council (Advanced Grant SiMoSoMa). This work is a part of the research program of the Stichting voor Fundamenteel Onderzoek der Materie, which is financially supported by the Netherlands Organization for Scientific Research. We thank H. van der Meer for precious help with the experimental setup.

Supporting Online Material

www.sciencemag.org/cgi/content/full/330/6002/353/DC1
Materials and Methods
Figs. S1 to S9
References

22 July 2010; accepted 16 September 2010
10.1126/science.1195475

Atmospheric CO_2: Principal Control Knob Governing Earth's Temperature

Andrew A. Lacis,* Gavin A. Schmidt, David Rind, Reto A. Ruedy

Ample physical evidence shows that carbon dioxide (CO_2) is the single most important climate-relevant greenhouse gas in Earth's atmosphere. This is because CO_2, like ozone, N_2O, CH_4, and chlorofluorocarbons, does not condense and precipitate from the atmosphere at current climate temperatures, whereas water vapor can and does. Noncondensing greenhouse gases, which account for 25% of the total terrestrial greenhouse effect, thus serve to provide the stable temperature structure that sustains the current levels of atmospheric water vapor and clouds via feedback processes that account for the remaining 75% of the greenhouse effect. Without the radiative forcing supplied by CO_2 and the other noncondensing greenhouse gases, the terrestrial greenhouse would collapse, plunging the global climate into an icebound Earth state.

It often is stated that water vapor is the chief greenhouse gas (GHG) in the atmosphere. For example, it has been asserted that "about 98% of the natural greenhouse effect is due to water vapour and stratiform clouds with CO_2 contributing less than 2%" (*1*). If true, this would imply that changes in atmospheric CO_2 are not important influences on the natural greenhouse capacity of Earth, and that the continuing increase in CO_2 due to human activity is therefore not relevant to climate change. This misunderstanding is resolved through simple examination of the terrestrial greenhouse.

The difference between the nominal global mean surface temperature (T_S = 288 K) and the global mean effective temperature (T_E = 255 K) is a common measure of the terrestrial greenhouse effect ($G_T = T_S - T_E$ = 33 K). Assuming global energy balance, T_E is also the Planck radiation equivalent of the 240 W/m^2 of global mean solar radiation absorbed by Earth.

The Sun is the source of energy that heats Earth. Besides direct solar heating of the ground, there is also indirect longwave (LW) warming arising from the thermal radiation that is emitted by the ground, then absorbed locally within the atmosphere, from which it is re-emitted in both upward and downward directions, further heating the ground and maintaining the temperature gradient in the atmosphere. This radiative interaction is the greenhouse effect, which was first discovered by Joseph Fourier in 1824 (*2*), experimentally verified by John Tyndall in 1863 (*3*), and quantified by Svante Arrhenius in 1896 (*4*). These studies established long ago that water vapor and CO_2 are indeed the principal terrestrial GHGs. Now, further consideration shows that CO_2 is the one that controls climate change.

CO_2 is a well-mixed gas that does not condense or precipitate from the atmosphere. Water vapor and clouds, on the other hand, are highly active components of the climate system that respond rapidly to changes in temperature and air pressure by evaporating, condensing, and precipitating. This identifies water vapor and clouds as the fast feedback processes in the climate system.

Radiative forcing experiments assuming doubled CO_2 and a 2% increase in solar irradiance (*5*) show that water vapor provides the strongest climate feedback of any of the atmospheric GHGs, but that it is not the cause (forcing) of global cli-

NASA Goddard Institute for Space Studies, 2880 Broadway, New York, NY 10025, USA.

*To whom correspondence should be addressed. E-mail: andrew.a.lacis@nasa.gov

mate change. The response of the climate system to an applied forcing is determined to be the sum of the direct (no-feedback) response to the applied forcing and the induced radiative response that is attributable to the feedback process contributions. The ratio of the total climate response to the no-feedback response is commonly known as the feedback factor, which incorporates all the complexities of the climate system feedback interactions. For the doubled CO_2 and the 2% solar irradiance forcings, for which the direct no-feedback responses of the global surface temperature are 1.2° and 1.3°C, respectively, the ~4°C surface warming implies respective feedback factors of 3.3 and 3.0 (*5*).

Because the solar-thermal energy balance of Earth [at the top of the atmosphere (TOA)] is maintained by radiative processes only, and because all the global net advective energy transports must equal zero, it follows that the global average surface temperature must be determined in full by the radiative fluxes arising from the patterns of temperature and absorption of radiation. This then is the basic underlying physics that explains the close coupling that exists between TOA radiative fluxes, the greenhouse effect, and the global mean surface temperature.

An improved understanding of the relative importance of the different contributors to the greenhouse effect comes from radiative flux experiments that we performed using Goddard Institute for Space Studies (GISS) ModelE (*6*). Figure 1 depicts the essence of these calculations, including the separation of the greenhouse contributors into feedback and forcing categories.

In round numbers, water vapor accounts for about 50% of Earth's greenhouse effect, with clouds contributing 25%, CO_2 20%, and the minor GHGs and aerosols accounting for the remaining 5%. Because CO_2, O_3, N_2O, CH_4, and chlorofluorocarbons (CFCs) do not condense and precipitate, noncondensing GHGs constitute the key 25% of the radiative forcing that supports and sustains the entire terrestrial greenhouse effect, the remaining 75% coming as fast feedback contributions from water vapor and clouds.

We used the GISS 4° × 5° ModelE to calculate changes in instantaneous LW TOA flux (annual global averages) in experiments where atmospheric constituents (including water vapor, clouds, CO_2, O_3, N_2O, CH_4, CFCs, and aerosols) were added to or subtracted from an equilibrium atmosphere with a given global temperature structure, one constituent at a time for a 1-year period. Decreases in outgoing TOA flux for each constituent relative to the empty or the full-component atmosphere define the bounds for the relative impact on the total greenhouse effect. Had the overlapping absorption been negligible, the sum of the flux differences would have been equal to the LW flux equivalent of the total greenhouse effect ($G_F = \sigma T^4_S - \sigma T^4_E = 150$ W/m^2), where σ is the Stefan-Boltzmann constant. We found the single-addition flux differences to be overestimated by a factor of 1.36, whereas in the single-subtraction cases, the sum of the TOA flux differences was underestimated by a factor of 0.734. By normalizing these fractional contributions to match the full-atmosphere value of G_F, we obtained the fractional response contributions shown in Fig. 1.

Because of overlapping absorption, the fractional attribution of the greenhouse effect is to some extent qualitative (as shown by the dashed and dotted extremum lines in Fig. 1), even though the spectral integral is a full and accurate determination of the atmospheric greenhouse strength for the specified global temperature structure. Still, the fractional attribution is sufficiently precise to clearly differentiate the radiative flux contributions due to the noncondensable GHGs from those arising from the fast feedback processes. This allows an empirical determination of the climate feedback factor as the ratio of the total global flux change to the flux change that is attributable to the radiative forcing due to the noncondensing GHGs. This empirical determination leads then to a climate feedback factor of 4, based on the noncondensing GHG forcing accounting for 25% of the outgoing flux reduction at the TOA for the full-constituent atmosphere. This implies that Earth's climate system operates with strong positive feedback that arises from the forcing-induced changes in the condensable species.

A direct consequence of this combination of feedback by the condensable and forcing by the noncondensable constituents of the atmospheric greenhouse is that the terrestrial greenhouse effect would collapse were it not for the presence of these noncondensing GHGs. If the global atmospheric temperatures were to fall to as low as $T_S = T_E$, the Clausius-Clapeyron relation would imply that the sustainable amount of atmospheric water vapor would become less than 10% of the current atmospheric value. This would result in (radiative) forcing reduced by ~30 W/m^2, causing much of the remaining water vapor to precipitate, thus enhancing the snow/ice albedo to further diminish the absorbed solar radiation. Such a condition would inevitably lead to runaway glaciation, producing an ice ball Earth.

Claims that removing all CO_2 from the atmosphere "would lead to a 1°C decrease in global warming" (*7*), or "by 3.53°C when 40% cloud cover is assumed" (*8*) are still being heard. A clear demonstration is needed to show that water vapor and clouds do indeed behave as fast feedback processes and that their atmospheric distributions are regulated by the sustained radiative forcing due to the noncondensing GHGs. To this end, we performed a simple climate experiment with the GISS 2° × 2.5° AR5 version of ModelE, using the Q-flux ocean with a mixed-layer depth of 250 m, zeroing out all the noncondensing GHGs and aerosols.

The results, summarized in Fig. 2, show unequivocally that the radiative forcing by noncondensing GHGs is essential to sustain the atmospheric temperatures that are needed for significant levels of water vapor and cloud feedback. Without this noncondensable GHG forcing, the physics of this model send the climate of Earth plunging rapidly and irrevocably to an icebound state, though perhaps not to total ocean freezeover.

The scope of the climate impact becomes apparent in just 10 years. During the first year alone, global mean surface temperature falls by 4.6°C. After 50 years, the global temperature stands at –21°C, a decrease of 34.8°C. Atmospheric water vapor is at ~10% of the control climate value (22.6 to 2.2 mm). Global cloud cover increases from its 58% control value to more than 75%, and the global sea ice fraction goes from 4.6% to 46.7%, causing the planetary albedo of Earth to also increase from ~29% to 41.8%. This has the effect of reducing the absorbed solar energy to further exacerbate the global cooling.

After 50 years, a third of the ocean surface still remains ice-free, even though the global surface temperature is colder than –21°C. At tropical latitudes, incident solar radiation is sufficient to keep the ocean from freezing. Although this thermal oasis within an otherwise icebound Earth

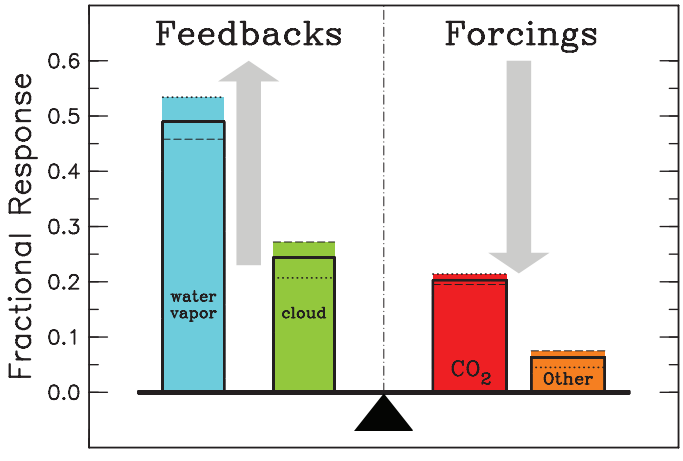

Fig. 1. Attribution of the contributions of individual atmospheric components to the total terrestrial greenhouse effect, separated into feedback and forcing categories. Horizontal dotted and dashed lines depict the fractional response for single-addition and single-subtraction of individual gases to an empty or full-component reference atmosphere, respectively. Horizontal solid black lines are the scaled averages of the dashed- and dotted-line fractional response results. The sum of the fractional responses adds up to the total greenhouse effect. The reference atmosphere is for conditions in 1980.

appears to be stable, further calculations with an interactive ocean would be needed to verify the potential for long-term stability. The surface temperatures in Fig. 3 are only marginally warmer than 1°C within the remaining low-latitude heat island.

From the foregoing, it is clear that CO_2 is the key atmospheric gas that exerts principal control over the strength of the terrestrial greenhouse effect. Water vapor and clouds are fast-acting feedback effects, and as such are controlled by the radiative forcings supplied by the noncondensing GHGs. There is telling evidence that atmospheric CO_2 also governs the temperature of Earth on geological time scales, suggesting the related question of what the geological processes that control atmospheric CO_2 are. The geological evidence of glaciation at tropical latitudes from 650 to 750 million years ago supports the snowball Earth hypothesis (*9*), and by inference, that escape from the snowball Earth condition is also achievable.

On million-year time scales, volcanoes are the principal source of atmospheric CO_2, and rock weathering is the principal sink, with the biosphere acting as both source and sink (*10*). Because the CO_2 sources and sinks operate independently, the atmospheric level of CO_2 can fluctuate. If the atmospheric CO_2 level were to fall below its critical value, snowball Earth conditions can result.

Antarctic and Greenland ice core data show atmospheric CO_2 fluctuations between 180 to 300 parts per million (ppm) over the glacial-interglacial cycles during the past 650,000 years (*11*). The relevant physical processes that turn the CO_2 control knob on thousand-year time scales between glacial and interglacial extremes are not fully understood, but appear to involve both the biosphere and the ocean chemistry, including a significant role for Milankovitch variations of the Earth-orbital parameters.

Besides CO_2, methane is another potent greenhouse control knob, being implicated in the Paleocene-Eocene thermal maximummass extinction 55 million years ago, when global warming by up to 5°C (*12*) occurred because of a massive release of methane from the disintegration of seafloor clathrates (*13*, *14*). Methane is the second most important noncondensing GHG after CO_2. Of the 2.9 W/m^2 of GHG radiative forcing from 1750 to 2000, CO_2 contributed 1.5 W/m^2, methane 0.55 W/m^2, and CFCs 0.3 W/m^2, with the rest coming from N_2O and ozone (*15*). All of these increases in noncondensing GHG forcing are attributable to human activity (*16*).

Climate control knobs on the solar side of the energy balance ledger include the steady growth in luminosity since the beginning of the Solar System (from about 70% of present luminosity, depending on the postulated early solar mass loss), as hydrogen is consumed in nuclear reactions in the solar interior (*17*, *18*). Milankovitch variations of the Earth-orbital parameters, which alter the relative seasonal distribution as well as the intensity of incident solar radiation within the polar regions, are another important solar energy control knob that is intimately associated with glacial-interglacial cycles of climate change. For solar irradiance changes over the past several centuries, an increase by about 0.1 W/m^2 is inferred since the time of the Maunder minimum, based on trends in sunspot activity and other proxies (*19*).

Of the climate control knobs relevant to current climate, those on the solar side of the energy balance ledger show only negligible impact. Several decades of solar irradiance monitoring have not detected any long-term trends in solar irradiance beyond the 11-year oscillation associated with the solar sunspot cycle. Large volcanic

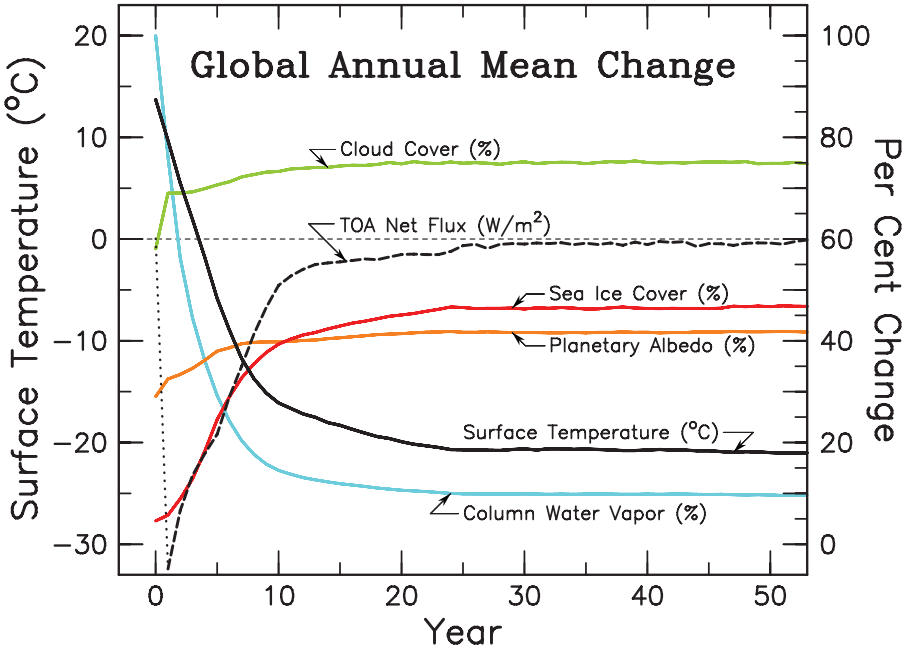

Fig. 2. Time evolution of global surface temperature, TOA net flux, column water vapor, planetary albedo, sea ice cover, and cloud cover, after the zeroing out of the noncondensing GHGs. The model used in the experiment is the GISS 2°× 2.5° AR5 version of ModelE, with the Q-flux ocean and a mixed-layer depth of 250 m. Model initial conditions are for a preindustrial atmosphere. Surface temperature and TOA net flux use the lefthand scale.

Fig. 3. Zonally averaged annual mean surface temperature change after the zeroing out of noncondensing GHGs.

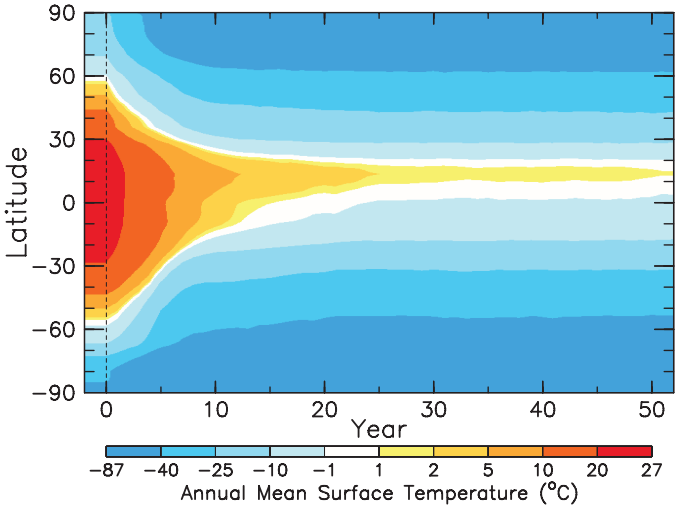

Table 1. Planetary greenhouse parameters.

Parameter	Mars	Earth	Venus
T_S (K)	215	288	730
T_E (K)	210	255	230
σT_S^4 (W/m^2)	121	390	16,100
σT_E^4 (W/m^2)	111	240	157
G_T (K)	5	33	500
G_F (W/m^2)	10	150	~16,000
P_S (bar)	0.01	1	100

eruptions can happen at any time, but no substantial eruptions have occurred since the eruption of Mt. Pinatubo in the Philippines in 1991.

In a broader perspective, CO_2 greenhouses also operate on Mars and Venus, because both planets possess atmospheres with substantial amounts of CO_2. The atmospheric greenhouse effect requires that a substantial fraction of the incident solar radiation must be absorbed at the ground in order to make the indirect greenhouse heating of the ground surface possible. Greenhouse parameters and relative surface pressure (P_S) for Mars, Earth, and Venus are summarized in Table 1.

Earth is unique among terrestrial planets in having a greenhouse effect in which water vapor provides strong amplification of the heat-trapping action of the CO_2 greenhouse. Also, N_2 and O_2, although possessing no substantial absorption bands of their own, are actually important contributors to the total greenhouse effect because of pressure-broadening of CO_2 absorption lines, as well as by providing the physical structure within which the absorbing gases can interact with the radiation field.

The anthropogenic radiative forcings that fuel the growing terrestrial greenhouse effect continue unabated. The continuing high rate of atmospheric CO_2 increase is particularly worrisome, because the present CO_2 level of 390 ppm is far in excess of the 280 ppm that is more typical for the interglacial maximum, and still the atmospheric CO_2 control knob is now being turned faster than at any time in the geological record (*20*). The concern is that we are well past even the 300- to 350-ppm target level for atmospheric CO_2, beyond which dangerous anthropogenic interference in the climate system would exceed the 25% risk tolerance for impending degradation of land and ocean ecosystems, sea-level rise, and inevitable disruption of socioeconomic and food-producing infrastructure (*21*, *22*). Furthermore, the atmospheric residence time of CO_2 is exceedingly long, being measured in thousands of years (*23*). This makes the reduction and control of atmospheric CO_2 a serious and pressing issue, worthy of real-time attention.

References and Notes

1. R. S. Lindzen, *Quart. J. R. Meteorol. Soc* **117**, 651 (1991).
2. J. Fourier, *Ann. Chemie Physique* **27**, 136 (1824).
3. J. Tyndall, *Philos. Mag.* **25**, 200 (1863).
4. S. Arrhrenius, *Philos. Mag.* **41**, 237 (1896).
5. J. Hansen *et al.*, *AGU Geophys. Monogr.* **29**, 130 (1984).
6. G. A. Schmidt *et al.*, *J. Clim.* **19**, 153 (2006).
7. J. Tomkin, *Phys. Today* **45**, 13 (1992).
8. R. S. Lindzen, H. Charnock, K. P. Shine, R. Kandel, *Phys. Today* **48**, 78 (1995).
9. J. L. Kirschvink, in *The Proterozoic Biosphere: A Multidisciplinary Study*, J. W. Schopf, C. Klein, D. Des Maris, Eds. (Cambridge Univ. Press, Cambridge, 1992), pp. 51–52.
10. R. A. Berner, *The Phanerozoic Carbon Cycle: CO_2 and O_2* (Oxford Univ. Press, New York, 2004).
11. E. Jansen *et al.*, in *Climate Change 2007: The Physical Science Basis. Contribution of Working Group I to the Fourth Assessment Report of the Intergovernmental Panel on Climate Change*, S. Solomon *et al.*, Eds. (Cambridge Univ. Press, Cambridge, 2007), pp. 433–497.
12. J. C. Zachos, G. R. Dickens, R. E. Zeebe, *Nature* **451**, 279 (2008).
13. G. R. Dickens, J. R. O'Neil, D. K. Rea, R. M. Owen, *Paleoceanography* **10**, 965 (1995).
14. G. A. Schmidt, D. T. Shindell, *Paleoceanography* **18**, 1004 (2003).
15. J. Hansen *et al.*, *J. Geophys. Res.* **110**, D18104 (2005).
16. K. L. Denman *et al.*, in *Climate Change 2007: The Physical Science Basis. Contribution of Working Group I to the Fourth Assessment Report of the Intergovernmental Panel on Climate Change*, S. Solomon *et al.*, Eds. (Cambridge Univ. Press, Cambridge, 2007), pp. 499–587.
17. I. J. Sackmann, A. I. Boothroyd, K. E. Kraemer, *Astrophys. J.* **418**, 457 (1993).
18. I. J. Sackmann, A. I. Boothroyd, *Astrophys. J.* **583**, 1024 (2003).
19. P. Forster *et al.*, in *Climate Change 2007: The Physical Science Basis. Contribution of Working Group I to the Fourth Assessment Report of the Intergovernmental Panel on Climate Change*, S. Solomon *et al.*, Eds. (Cambridge Univ. Press, Cambridge, 2007), pp. 433–497.
20. D. Archer *et al.*, *Annu. Rev. Earth Planet. Sci.* **37**, 117 (2009).
21. L. D. D. Harvey, *Clim. Change* **82**, 1 (2007).
22. J. Hansen *et al.*, *Open Atmos. Sci. J.* **2**, 217 (2008).
23. F. Joos, R. Spahni, *Proc. Natl. Acad. Sci. U.S.A.* **105**, 1425 (2008).

24. We thank B. Carlson, A. Del Genio, J. Hansen, G. Russell, R. Stothers, and L. Travis for comments and the NASA Earth Science Research Division managed by J. Kaye and D. Considine for support.

Supporting Online Material

www.sciencemag.org/cgi/content/full/330/6002/356/DC1
SOM Text
Figs. S1 and S2
Table S1
References

8 April 2010; accepted 10 September 2010
10.1126/science.1190653

The Structure of Iron in Earth's Inner Core

Shigehiko Tateno,[1,2]* Kei Hirose,[1,2]* Yasuo Ohishi,[3] Yoshiyuki Tatsumi[2]

Earth's solid inner core is mainly composed of iron (Fe). Because the relevant ultrahigh pressure and temperature conditions are difficult to produce experimentally, the preferred crystal structure of Fe at the inner core remains uncertain. Static compression experiments showed that the hexagonal close-packed (hcp) structure of Fe is stable up to 377 gigapascals and 5700 kelvin, corresponding to inner core conditions. The observed weak temperature dependence of the *c*/*a* axial ratio suggests that hcp Fe is elastically anisotropic at core temperatures. Preferred orientation of the hcp phase may explain previously observed inner core seismic anisotropy.

Determining the crystal structure of iron (Fe) under ultrahigh pressure and temperature (*P*-*T*) conditions is a key piece of information required to decipher the complex seismic structures observed in Earth's inner core (*1*–*3*). Fe adopts body-centered cubic (bcc) structure at ambient conditions and transforms into the hexagonal close-packed (hcp) phase above 15 GPa. Although hcp Fe can persist under core pressures at 300 K (*4*, *5*), a phase transition at elevated temperature is a possibility. Both theory and experiments have proposed different forms of Fe at simultaneously high *P*-*T* conditions, which include bcc (*6*, *7*), face-centered-cubic (fcc) (*8*), and hcp structures (*5*, *9*). The structure of Fe has never been examined experimentally at the inner core *P*-*T* conditions (>330 GPa and ≥5000 K), because the techniques previously used to produce such extreme conditions—dynamical shock-wave experiments—impede the ability to make simultaneous structure measurements on the order of a microsecond.

Based on a combination of static compression experiments in a laser-heated diamond-anvil cell (DAC) and synchrotron x-ray diffraction (XRD) measurements (Fig. 1), we determined the structure of Fe up to 377 GPa and 5700 K (*10*). A temperature gradient was relatively large when the sample was heated to more than 5000 K at >300 GPa (Fig. 2A); nevertheless, the variations were less than ±10% in the 6-μm region across the hot spot, which corresponds to the x-ray beam size at full width at half maximum, considering the fluctuations in temperature with time (Fig. 2B). We calculated the sample temperature by averaging the variation in the 6-μm area probed by x-rays. Pressure was determined from the unit-cell volume of hcp Fe, using its *P*-*V*-*T* (where *V* is volume) equation of state (*11*). The ±10% temperature variation leads to about ±2% uncertainty in pressure (377 ± 8.5 GPa at 5700 K). The pressure gradient in the sample was <5 GPa at ~300 GPa in a 10-μm area after heating.

To construct the phase diagram of Fe at inner core conditions, we conducted six separate sets of experiments (Fig. 3). The first experiment at 303 GPa and room temperature resulted in an XRD pattern that included peaks from hcp Fe and Re (the gasket material) (fig. S1A) (*10*). Subsequently, we heated this sam-

[1]Department of Earth and Planetary Sciences, Tokyo Institute of Technology, Ookayama, Meguro, Tokyo 152-8551, Japan. [2]Institute for Research on Earth Evolution, Japan Agency for Marine-Earth Science and Technology, Yokosuka, Kanagawa 237-0061, Japan. [3]Japan Synchrotron Radiation Research Institute, Sayo, Hyogo 679-5198, Japan.

*To whom correspondence should be addressed. E-mail: tateno.s.aa@m.titech.ac.jp (S.T.); kei@geo.titech.ac.jp (K.H.)

Supporting Online Material for

Atmospheric CO_2: Principal Control Knob Governing Earth's Temperature

Andrew A. Lacis[1,#], Gavin A. Schmidt[1], David Rind[1], Reto A. Ruedy[1]

[1]NASA Goddard Institute for Space Studies 2880 Broadway, New York, NY 10025.
[#]To whom all correspondence should be addressed.

In climate GCMs, radiative calculations are typically performed at every grid box once every two to three hours of simulated time. These model calculations account for the radiative properties, amount and vertical distribution of atmospheric gases, clouds, and aerosols, ground surface and atmospheric temperature, as well as the surface reflectivity and emissivity, solar zenith angle, and the Sun-Earth distance. Solar heating and LW cooling rates, the energy balance at ground, and at the top of the atmosphere (TOA) are the result of these radiative calculations that define the energy balance of the Earth, and also have a diagnostic role to document and assess the climate model performance.

Fractional attribution of how much each atmospheric gas contributes to the strength of the terrestrial greenhouse effect could in principle be calculated for any point in time and any specified instantaneous temperature and climate variable distribution. But, since the climate system is never in equilibrium, being driven by large diurnal and seasonal changes in solar irradiance, and large climate system responses that are disproportionate to the systematic variations of radiative forcing (producing overshooting fluctuations relative to the equilibrium climate reference point), interpretation of the calculated fluxes has to account for the disequilibrium conditions, requiring averaging over the omnipresent variability of atmospheric constituents.

It therefore is preferable to select a full year as the time interval over which longwave (LW) fluxes are to be averaged, since for this time interval, there is an expectation for global energy balance equilibrium. Still, there is natural inter-annual variability both in the real world and in climate GCM simulations. This produces a year to year variability of order 1 W/m^2 in the flux equivalent of the total greenhouse effect ($G_F = \sigma T^4_S - \sigma T^4_E$), where σ is the Stefan-Boltzmann constant, even for a model that has ostensibly come to equilibrium. Thus, to define the equilibrium value of G_F requires averaging model results over a substantially longer time period, or by utilizing appropriate normalization.

We have made use of the second option by normalizing the LW fluxes listed in Table S1 to yield a precise agreement with the global mean absorbed solar radiation, or equivalent of applying a 0.15 °C uniform atmospheric temperature change. Alternatively, we could have selected a model year that was in closer radiative equilibrium than the one used in a parallel radiative flux attribution study *(S1)*. As a result, we find G_F = 152.6 W/m^2 instead of the G_F = 153.4 W/m^2 value, which is the direct ModelE LW flux difference between the surface and TOA fluxes, reflecting the slight TOA flux imbalance resulting from the ongoing inter-annual variability.

The flux (or temperature) normalization is also applied to flux differences in Table S1 for ModelE experiment results to calculate the changes in instantaneous LW TOA flux (annual global means) in experiments where atmospheric constituents (water vapor, cloud, CO_2, O_3, N_2O, CH_4, CFCs and aerosols) were added and subtracted one at a time relative to an empty (single-addition) or full component (group-subtraction) reference atmosphere.

Because of overlapping absorption, flux changes in the single-addition column sum to G_F = 206.8 W/m^2 instead of G_F = 152.6 W/m^2, which would be the full strength of the terrestrial equilibrium greenhouse effect. Meanwhile, for the group-subtraction cases, individual component flux changes sum to G_F = 112.0 W/m^2 instead of the G_F = 152.6 W/m^2 full atmosphere reference value. Along side are the fractional changes for both sets of experiments. The overlapping absorption is spectral and as well as spatial, hence the differences in fractional contributions. Since the group-subtraction values are somewhat closer to the equilibrium G_F value, they need to be weighted more heavily. Thus, by taking 0.572 times the group-subtraction values, and 0.428 times the single-addition values, we arrive at the normalized average fractional contributions listed in the right-hand column of Table S1, with the equivalent radiative fluxes to the left. These normalized fractions were used to construct Fig. 1. As has been stressed, while the fractional attribution is to some extent imprecise, it is robust in that the sum of all of the contributing pieces must be equal to the total flux equivalent greenhouse strength G_F, which is numerically accurately defined. Climate GCMs that can accurately simulate current climate will produce similar fractional attribution for the principal climate variables listed in Table S1.

Having emphasized that the global energy balance of Earth is fully described in terms of the solar and LW radiative fluxes, including the fractional attribution among contributing atmospheric constituents, it should be noted that the atmospheric temperature gradient (lapse rate) has direct impact on the radiative properties of the atmosphere, and is therefore a key factor in determining the magnitude of the greenhouse effect. Energy transport by convective and advective means helps define the global atmospheric temperature structure. Climate models are specifically designed to reproduce the atmospheric motions in three dimensions in order to generate realistic temperature profiles that are needed for the radiative model calculations to obtain reliable radiative heating-cooling rates and fluxes.

Table S1. Single-addition & group-subtraction LW flux changes

LW absorber	single-addition		group-subtraction		normalized average	
	Wm^{-2}	fraction	Wm^{-2}	fraction	Wm^{-2}	fraction
H_2O	94.7	.458	59.8	.534	74.7	.490
cloud	56.2	.272	23.2	.207	37.3	.244
CO_2	40.3	.195	24.0	.214	31.0	.203
O_3	4.0	.019	1.7	.015	2.7	.018
N_2O	4.1	.020	1.5	.013	2.6	.017
CH_4	3.5	.017	1.2	.011	2.2	.014
CFCs	1.0	.005	0.2	.002	0.6	.004
aerosol	3.0	.014	0.4	.004	1.5	.010
sum	206.8	1.000	112.0	1.000	152.6	1.000

Under prevailing climate conditions, the temperature equivalent greenhouse strength is G_T = 33.2 °C, and the flux equivalent value is G_F = 152.6 W/m^2. It is also for this current climate temperature structure that the flux attribution between condensable (feedback) and the non-condensable (forcing) species enables the empirical determination of the overall climate system feedback factor of 4. This is in contrast to the climate feedback sensitivity for small perturbations relative to current climate (e.g., 3 °C for doubled CO_2) that yield a feedback factor of ~2.5. But, by taking into account the (~1.2 °C) negative feedback due to moist convective lapse rate change, we obtain a feedback factor of 3.5, more compatible in magnitude (for the same method of evaluation) to the overall climate system value of 4. As recently pointed out by Aires and Rossow *(S2)*, the climate system feedback interactions are non-linear and the feedback sensitivities are state-dependent and therefore variable with time, and thus are not 'constants' of the climate system.

A further perspective on the effect of the atmospheric lapse rate on the greenhouse strength comes from radiative equilibrium (RE) calculations. If energy transport is by radiative means only, the global equilibrium surface temperature is 321 K, instead of the nominal 288 K value under conditions of radiative-convective equilibrium (RCE). This results in $G_{T,RCE}$ = 33 °C, and $G_{T,RE}$ = 66 °C, for the strength of the terrestrial greenhouse effect with and without convective-advective energy transport, a result obtained previously by Manabe and Moller *(S3)* in the early days of 1-D climate modeling.

The above results show that in greenhouse attribution, lapse rate contributions need to be properly accounted for, and that because of overlapping absorption, small ambiguities persist in the precise fractional attribution of flux contributions. However, the key concept separating and quantifying the condensable (feedback) and non-condensable (forcing) contributions by the different climate system components is robust, fully confirming CO_2 as the strongest radiative forcing agent in the atmosphere. Also, as shown in Figs. S1 and S2, model results obtained with the coupled atmosphere-ocean model, except for the order of magnitude longer time constant, are very similar to the Q-flux ocean model results, again confirming that CO_2 control of global climate is a decidedly atmospheric effect.

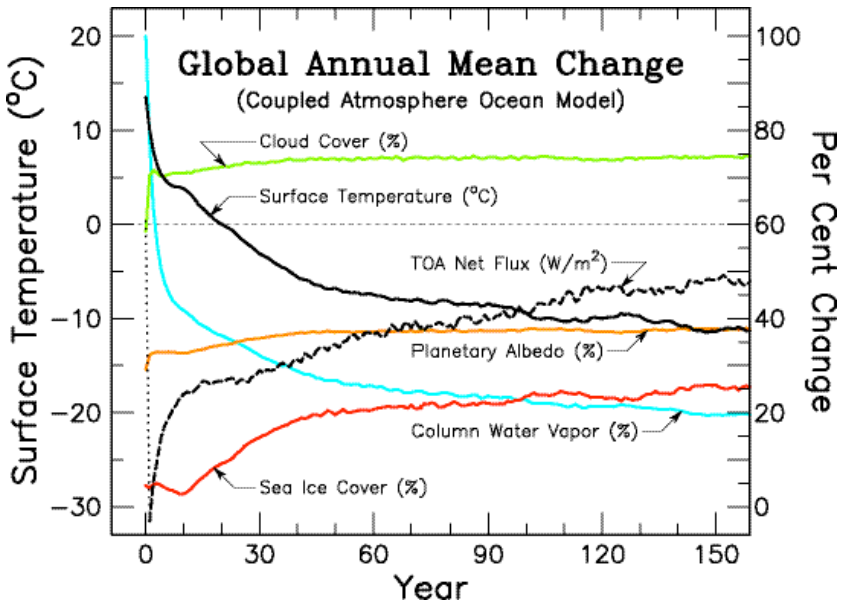

Fig. S1. Time evolution of global surface temperature, TOA net flux, column water vapor, planetary albedo, sea ice cover, and cloud cover, following the zeroing out of the non-condensing greenhouse gases. The model used in the experiment is the GISS 2°× 2.5° AR5 version of ModelE with coupled atmosphere-ocean. The model initial conditions are for a pre-industrial atmosphere. Surface temperature and TOA net flux use the left-hand scale. The run stopped because of a local diagnostic check due to ice freezing reaching the bottom of the ocean after 160 years of simulated time.

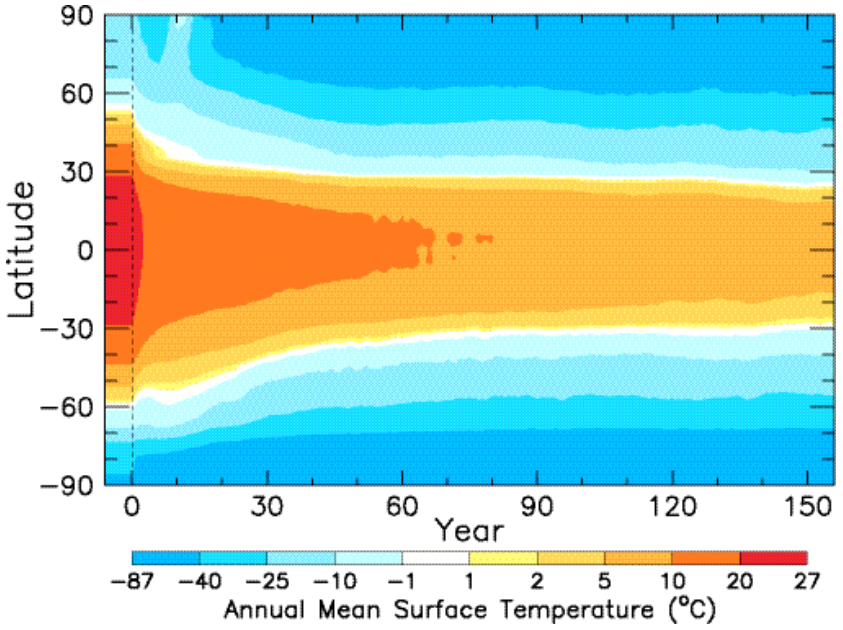

Fig. S2. Zonally averaged annual-mean surface temperature change following the zeroing out of non-condensing greenhouse gases. Model particulars are as described in Fig. S1. The main effect of the coupled atmosphere-ocean model compared to the Q-flux ocean model is the order of magnitude longer time scale for the interactive ocean to reach equilibrium. Since the CO_2 radiative forcing control of global climate is an atmospheric effect, there is no significant difference in the end result.

References

S1. G. A. Schmidt *et al.*, *J. Geophys. Res.* **115**, doi:10.1029/2010JD014287, (2010).

S2. F. Aires and W.B. Rossow, *Q. J. Royal Meteorol. Soc.* **129**, 239, (2003).

S3. S. Manabe and F. Moller, *Monthly Weather Rev.* **89**, 503, (1961).